HHS Public Access

Author manuscript

Nature. Author manuscript; available in PMC 2022 September 09.

Published in final edited form as:

Nature. 2021 September ; 597(7875): 274–278. doi:10.1038/s41586-020-2931-3.

Defining HPV-specific B cell responses in head and neck cancer patients

Andreas Wieland[1,2,*], **Mihir R. Patel**[3,4], **Maria A. Cardenas**[5], **Christiane S. Eberhardt**[1,2], **William H. Hudson**[1,2], **Rebecca C. Obeng**[1,2,6], **Christopher C. Griffith**[4,6], **Xu Wang**[7], **Zhuo G. Chen**[7], **Haydn T. Kissick**[1,2,4,5], **Nabil F. Saba**[4,7], **Rafi Ahmed**[1,2,4,*]

[1]Emory Vaccine Center, Emory University School of Medicine, Atlanta, GA, USA

[2]Department of Microbiology & Immunology, Emory University School of Medicine, Atlanta, GA, USA

[3]Department of Otolaryngology, Emory University School of Medicine, Atlanta, GA, USA

[4]Winship Cancer Institute of Emory University, Atlanta, GA, USA

[5]Department of Urology, Emory University School of Medicine, Atlanta, GA, USA

[6]Department of Pathology, Emory University School of Medicine, Atlanta, GA, USA

[7]Department of Hematology & Medical Oncology, Emory University School of Medicine, Atlanta, GA, USA

SUMMARY

Tumours can harbour significant numbers of B cells and plasma cells, however, little is known about the antigen specificity of intra-tumoral B cells[1–8]. Here we show that human papillomavirus (HPV)-specific B cell responses are detectable in HPV-positive head and neck cancers, with active production of HPV-specific IgG antibodies in situ. HPV-specific antibody secreting cells (ASCs) were readily detectable (~0.7-25% of IgG+ ASCs) in the tumour microenvironment (TME) with minimal bystander recruitment of influenza-specific cells, suggesting a localised and antigen-specific ASC response. HPV-specific ASC responses, which correlated with plasma IgG titres, were directed against the HPV proteins E2, E6, and E7, with E2-specific responses tending to be the most dominant. Using intra-tumoral B cells and plasma cells, we generated several HPV-

*corresponding authors: Material requests and correspondence should be directed to Rafi Ahmed (rahmed@emory.edu) or Andreas Wieland (andreas.wieland@emory.edu).

Contributions A.W. conceived and designed the project. A.W. and R.A. designed experiments and wrote the manuscript. A.W. performed most of the experiments (including cell isolation, ELISPOT, serology, flow cytometry and mAb generation) and analysed the generated data. C.S.E. performed MBC assays and helped with flow cytometry experiments. M.A.C. and H.T.K analysed scRNAseq data. W.H.H. analysed bulk RNAseq data. R.C.O. performed and analysed mIHC experiments. M.R.P. collected and provided human specimens, and analysed patient data. C.C.G. and X.W. handled human specimens. N.F.S. and Z.G.C. initiated the clinical specimen protocol. All authors contributed to the revision of the manuscript.

Materials HPV-specific mAbs are available with a completed Material Transfer Agreement.

Competing interests A.W. and R.A. are inventors on a patent filed by Emory University relating to HPV-specific mAbs and HPV E2 as potential immunological target in HPV-positive cancers. All other authors declare no competing interests.

Code availability

Custom code for RNA-seq and scRNA-seq are available from the corresponding authors upon reasonable request.

specific human monoclonal antibodies, which exhibited a high degree of somatic hypermutation, consistent with chronic antigen exposure. scRNAseq analyses revealed the presence of activated B cells, germinal centre B cells, and ASCs within the TME. ASCs and B cells were preferentially localised in the tumour stroma, with well-formed clusters of activated B cells indicating ongoing germinal centre reactions. Overall, we show that antigen-specific activated and germinal centre B cells as well as plasma cells can be found in the TME. Our findings provide a better understanding of humoral immune responses in human cancer and suggest that tumour-infiltrating B cells could be harnessed for the development of novel therapeutic agents.

INTRODUCTION

Tumours can harbour significant infiltrations of B cells and plasma cells, however, the role of tumour-infiltrating B cells lineage is not well defined[1–8]. Little is known about the antigen specificity of B cells and antibody-secreting cells (ASCs) in the tumour microenvironment (TME), which could partially explain the controversial findings regarding the role of B cells in several studies. Here we investigated the humoral immune response in the TME of human papillomavirus (HPV)-positive head and neck squamous cell carcinoma (HNSCC) patients with regards to its antigen specificity.

HPV-specific ASCs are present in the TME

We obtained surgically resected HNSCC samples expressing p16, a widely-used surrogate marker for HPV status, especially in oropharyngeal squamous cell carcinoma[9]. We confirmed HPV status using genomic DNA isolated from FFPE sections of 32 p16+ HNSCC patients of our cohort (n=43). HPV DNA was detected in 31 out of 32 samples with the vast majority of cases (84.4%) testing positive for HPV type 16 (Extended Data Fig. 1a), in agreement with previous reports[9–11]. We next set out to quantify total ASCs in tumour-infiltrating lymphocytes of primary tumours (TIL), metastatic lymph nodes (metLN), and peripheral blood mononuclear cells (PBMC) isolated from p16+ HNSCC patients. Compared to PBMCs, metLN and TIL showed a marked enrichment of ASCs (Extended Data Fig. 1b–e). ASCs in metLN and TIL predominantly produced IgG followed by IgA and IgM, with IgG+ ASCs accounting for 0.11% to 3.8% of total lymphocytes. In contrast, ASCs in the peripheral blood of p16+ HNSCC patients were less frequent and showed a different isotype distribution (IgA≥IgG>IgM), comparable in terms of frequency and isotype distribution to peripheral blood ASCs of healthy individuals[12].

We next sought to address the question whether ASCs in the TME produce antibodies specific for HPV antigens. Due to the high prevalence of IgG+ ASCs in the TME, we focused our efforts on antigen-specific IgG+ ASCs using the classical HPV oncogenes E6 and E7 as well as the regulatory protein E2. In contrast to cervical cancer, E2 is expressed in the majority of HPV-associated HNSCC due to episomal maintenance of the HPV genome[10]. IgG+ ASCs producing antibodies specific for E2, E6 and E7 were readily detectable in metLN and TIL with individual antigen responses accounting for up to 20% of total IgG+ ASCs (Fig. 1a–c and Extended Data Fig. 1f). E2-specific responses tended to be the most dominant among the tested antigens. The frequencies of HPV-specific IgG+ ASCs in 18 patient-matched metLN and TIL samples correlated (Extended Data Fig. 1g). Of

note, HPV-specific ASCs were undetectable in the peripheral blood suggesting a localised ASC response (Extended Data Fig. 1f). p16- HNSCC tumours, which, consistent with previous reports[13], exhibited significantly reduced lymphocyte infiltration compared to p16+ tumours, showed comparable frequencies of total ASCs but lacked HPV-specific IgG+ ASCs (Extended Data Fig. 2a–c). In line with the absence of HPV-specific ASC responses in the TME, HPV-specific IgG+ memory B cells (MBCs) were absent in almost all analysed (8/9) p16- HNSCC patients but readily detectable in the circulation of p16+ HNSCC patients (n=27) (Fig. 1d, Extended Data Fig. 2d).

We next compared the frequency of influenza- and HPV-specific ASCs in the TME of 14 p16+ HNSCC patients to exclude the possibility that the presence of HPV-specific IgG+ ASCs in the TME simply reflects inflammation-driven recruitment and differentiation of circulating MBCs. While influenza-specific MBCs were strikingly higher in peripheral blood (~1-2% vs. 0.2%), HPV-specific ASCs dominated in the TME (~2% vs. 0.2%) (Fig. 1d,e). These data suggest that, while some level of bystander recruitment or activation of unrelated antigen specificities such as influenza might occur, HPV-specific ASC responses in the TME are mainly antigen-driven. Overall, we show that HPV-specific IgG antibodies are actively produced in the TME with the E2 protein being a major target of the humoral immune response.

Correlation between ASC and HPV antibody

The presence of HPV-specific IgG+ ASCs in the TME prompted us to investigate the serological response to HPV E2/6/7 in our cohort. In accordance with recent studies[14–16], plasma IgG antibody titres against E2/6/7 could clearly distinguish p16+ (n=39) from p16- HNSCC patients (n=10) and healthy individuals (n=50) (Fig. 2a, Extended Data Fig. 3a–c). In contrast, IgA and IgM antibody titres against E2/6/7 were mostly absent or low (Extended Data Fig. 3d,e). Overall, IgG antibody titres to E2 tended to be highest, followed by E6- and E7-specific antibodies, with the majority of p16+ HNSCC patients having detectable antibody titres against all 3 antigens and the vast majority against at least 2 antigens (Extended Data Fig. 3f,g). The plasma IgG response to HPV E antigens predominantly consisted of IgG1, followed by highly variable levels of IgG3 in a subset of patients (Fig. 2b). In contrast, antibodies of the IgG2 and IgG4 subclasses were undetectable in the vast majority of patients. Interestingly, HPV-specific IgG titres correlated with the frequencies of HPV-specific IgG+ ASCs in metLN (n=30) as well as TIL (n=18) (Fig. 2c, Extended Data Fig. 3h).

Generation of HPV-specific human mAbs

We have previously identified a subset of antigen-specific B cells termed ‘activated B cells’ (ABCs), which are proliferating cells distinct from ASCs, committed to the MBC lineage and present in the peripheral blood following vaccination or infection[17]. We next asked whether HPV-specific ABCs are present in the TME and could be harnessed for the generation of HPV-specific human monoclonal antibodies (mAbs). We used fluorescently-labelled E2 protein to FACS-purify HPV-specific ABCs ($CD19^{+}IgD^{-}CD20^{+}CD71^{+}$) from a HPV+ metLN, followed by the generation of mAbs (Fig. 3a). 12 out of 14 successfully generated mAbs (~86%) recognised E2 in an ELISA (Fig. 3b). Furthermore,

we obtained an additional E2-specific mAb (22-1B10) from single-cell sorted ASCs ($CD19^+IgD^-CD20^-CD71^+$). E2-specific mAbs exhibited a high degree of somatic hypermutation (SHM) in the variable region of heavy (VH) and light (VL) chain with 3 clonal lineages being represented by 2 clones each (Fig. 3c). The VH of E2-specific mAbs harboured on average 28 SHMs, which is strikingly higher compared to mAbs generated in response to acute viral infections such as Ebola[18], latent viral infections such as varicella-zoster[19], or repeated antigenic exposures such as influenza[17,20]. The high degree of SHM of E2-specific mAbs is comparable to HIV-specific mAbs, which carry on average up to ~30 SHMs, although HIV-specific mAbs can harbour up to 70 SHMs[21]. The generated mAbs recognised several distinct non-overlapping epitopes of the E2 protein (Extended Data Fig. 4a). In addition to E2-specific mAbs, we also cloned 3 E6-specific mAbs from single cell sorted ASCs from another metLN, which also displayed a high degree of SHM (Extended Data Fig. 4b,c). Our data clearly demonstrate the presence of ABCs and ASCs specific for tumour-associated viral antigens in the TME. Furthermore, the presence of ABCs and the high degree of SHM among HPV-specific mAbs suggest a prolonged and ongoing humoral immune response to these tumour-associated viral antigens.

scRNA-seq analysis of B cells in the TME

To interrogate the composition of activated cells of the B cell lineage ($CD19^+IgD^-CD71^+$) in the TME in an unsupervised manner, we performed scRNA-seq on FACS-purified cells obtained from metLN and TIL of 3 HPV+ HNSCC patients (Fig. 4a). In addition, we also isolated activated cells from the peripheral blood of an influenza vaccinee 7 days post vaccination. The analysis of a total of 8,271 single cells identified 4 clusters (Fig. 4b,c). Based on gene expression profiles and gene set enrichment analyses, we termed the cell clusters ABC, ASC, germinal centre B cells (GCB), and transitory cells (TC), which displayed a hybrid phenotype with ASC, GCB and proliferation gene sets being enriched (Extended Data Fig. 5a,b). The ABC and GCB clusters were characterised by expression of *MS4A1* (CD20) and *ID3*, with *GPR183* (EBI2) being absent in GCB consistent with its role in mediating egress from GCs[22] (Extended Data Fig. 5c). The ASC cluster was characterised by expression of *CD38*, *MZB1*, *PRDM1* (BLIMP-1), and *XBP1*, whereas GCBs expressed *TCL1A*, *AICDA*, and *MME* (CD10). In general, activated cells derived from metLN and TILs were found in all cell clusters, although the distribution varied substantially between patients (Fig. 4d, Extended Data Fig. 5d). In contrast, activated cells derived from PBMCs 7 days post seasonal influenza vaccination were not detected in the GCB cluster and virtually absent from the TC cluster. These data thus demonstrate that the TME encompasses several antigen-experienced B cell subsets, including ABCs, GCBs and ASCs.

Transcriptome of sorted B cell subsets

We next performed RNA-seq analyses to identify transcriptional differences between the 3 major B cell subsets identified (ASCs, ABCs, and GCBs). We FACS-purified ASCs ($CD19^+CD20^-IgD^-CD38^{hi}CD71^+$), ABCs ($CD19^+CD20^+IgD^-CD71^+CD10^-$), and GCBs ($CD10^+$ ABCs) from 2 metLNs and 2 TILs of HPV+ HNSCC patients (Fig. 5a). In addition, we also analysed ASCs and ABCs of an influenza vaccinee isolated from peripheral blood on day 7 post vaccination (Extended Data Fig. 6a,b). To broadly characterise the transcriptional landscape, we initially performed principal component analysis, which

identified two principal components (PC) that collectively explained ~60% of the observed transcriptional variance (Fig. 5b). PC_1 accounted for 41% of transcriptional variance, clearly distinguished ASCs, ABCs and GCBs, and also separated tissue from blood ABCs. Gene expression analysis of individual genes by *k*-means clustering identified 6 gene clusters, distinguishing the samples based on sorted subsets as well as the sample origin (blood versus tissue) (Fig. 5c, Supplementary Table 1). Independent of sample origin, ASCs were characterised by elevated expression of common ASC-associated genes such as *XBP1*, *MZB1*, *CD27*, and *CD38*, and low expression of B cell lineage genes such as *MS4A1* (CD20), *IRF8* and *CD24*[17]. Furthermore, tumour-derived ASCs showed increased expression of additional plasma cell-associated genes such as *PRDM1*, *SDC1* (CD138), and *CD9*[23,24]. Consistent with these data, the majority of ASCs in the TME (n=14) did not express Ki-67 (Extended Data Fig. 6c), suggesting a more plasma-cell like phenotype of tumour-associated ASCs. GCBs expressed high levels of *BCL6*, *AICDA*, *MME*, and *S1PR2*, which promotes confinement to GCs[25]. Of note, influenza-specific cells from peripheral blood differed from tumour-derived cells by high expression of genes involved in cell migration such *CD52*, *S1PR4*, and *ITGA3*.

B cells and plasma cells in the TME can inhibit anti-tumour immunity through various immunomodulatory proteins including, but not limited to, TGF-β, IL-10, and IL-35[4–6,26]. Of note, with the exception of ASCs expressing low to intermediate levels of *GZMB*, *IDO1,* and *TGFBI*, the majority of previously described immunomodulatory genes were expressed at undetectable or low levels, and comparable to naïve B cells (Extended Data Fig. 6d).

Intratumoral localisation of B cells

We next set out to investigate the localisation of B cells and ASCs in the TME of HPV+ HNSCC tumours (n=7) using multiplex immunohistochemistry (Fig. 5d, Extended Data Fig. 7a). Total B cells ($CD19^+CD20^+$) and ASCs ($CD19^+CD20^-IRF4^+$) were more prevalent in the stroma compared to the p16+ tumour parenchyma (Fig. 5e). Activated B cells ($CD19^+CD20^+Ki\text{-}67^+$) tended to be present at higher densities in the stroma, with well-formed clusters of ABCs, indicating germinal centre reactions, being present in tumour stroma (Fig. 5e). ASCs in the TME were predominantly $Ki\text{-}67^-$ but varied substantially in their expression of CD138, suggesting various stages of plasma cell differentiation (Extended Data Fig. 7b). Similar trends were observed in 3 HPV- HNSCC tumours, although B cell infiltration was about 10-fold lower, which is in line with overall reduced lymphocyte infiltration in HPV- tumours (Extended Data Fig. 7c). Overall, our data show that several distinct antigen-specific B cell subsets are present in the TME, including ABCs, GCBs, recently generated plasmablasts as well as plasma cells at various differentiation stages.

Discussion

Previous studies assessing the contribution of B cells to tumour immunosurveillance and their prognostic value have yielded conflicting data[1–8,27]. The underlying reasons for these discordant data are probably multifaceted, including insufficient information about the phenotype of tumour-infiltrating B cells, their spatial organisation or their antigen

specificity. The importance of spatial organisation has recently been demonstrated by several studies linking the presence of B cells, especially in the context of tertiary lymphoid structures, with overall favourable outcomes and response to immunotherapy[1–3,27]. However, little is known about the antigen specificity of B cells and ASCs in the TME, with the majority of data being derived from intratumoral B cell repertoire analyses, precluding functional information of tumour-reactive B cells and whether the respective antibodies are being actively secreted[26]. Here we demonstrate that HPV-specific B cells are present in HPV+ HNSCC with HPV-specific IgG antibodies being actively secreted in situ. HPV-specific antibodies showed a high degree of SHM, comparable to HIV-specific antibodies[21], suggesting prolonged antigen exposure, which is further supported by the presence of GCBs. However, whether these mutations translate into increased affinity or rather represent an excessive, futile extent of SHM caused by chronic antigen exposure and/or a dysregulated cytokine milieu requires further investigation.

B cells and plasma cells in the TME can inhibit anti-tumour immunity through multiple mechanisms, with IL-10 being proposed as major immunoregulator[4–6,26]. In line with a previous report in HNSCC[8], ASCs, ABCs and GCBs showed limited expression of immunoregulatory genes. Interestingly, class switching to IgA was shown to be a prerequisite for IL-10-producing plasma cells in a prostate cancer model[6]. whereas in our HNSCC cohort ~80-90% of ASCs produced IgG. However, functional assays are ultimately required to assess the overall immunoregulatory activity of distinct B cell subsets.

Immunotherapeutic approaches for HPV-associated cancers, including vaccination with peptides or viral vectors, mostly focus on eliciting responses against E6/7 due to the absence of E2 expression in the vast majority of HPV-associated cervical cancers[10,28]. However, based on the increasing incidence of HPV-associated HNSCC[29] and our data demonstrating E2 being a major immunological target, it might prove advantageous to include E2 in future vaccination strategies, especially as E2 is large and harbours more potential T cell epitopes than E6 and E7 combined. Of note, a recent study identified several E2-derived CD8 T cell epitopes in HPV+ HNSCC patients[30]. Furthermore, we have also identified several E2-derived CD8 T cell epitopes and detected substantial numbers of E2-specific CD8 T cells in the TME of HPV+ HNSCC patients (Eberhardt et al., manuscript in preparation).

The role of HPV-specific antibodies in HPV-associated cancers is not well understood. However, two studies have suggested that increased HPV-specific antibody titres are associated with improved survival and reduced risk of recurrence in HPV+ HNSCC[15,31]. Our data show a clear correlation of HPV-specific antibody titres with ASCs in the TME. It is thus tempting to speculate that the presence of HPV-specific ASCs in the TME might also be associated with improved clinical outcome. However, additional studies are required to address whether increased HPV-specific antibody titres are merely markers of a more vigorous anti-tumoral immune response or whether HPV-specific antibodies play a role in anti-tumour immunity. While antibodies specific for intracellular antigens, such as HPV E proteins, are unlikely to exert direct anti-tumour effects through antibody-dependent cellular phagocytosis or cytotoxicity, they might contribute to anti-tumour immunity through indirect effects such as enhanced crosspresentation[32]. Antibodies against HPV antigens might thus contribute to the generation and maintenance of HPV-specific T cell responses. Overall,

these findings warrant the evaluation of antibodies targeting HPV E2/6/7, either in their native form or modified forms allowing increased access to intracellular compartments, as potential therapeutic treatment options for HPV-associated cancers.

Methods

Sample collection, preparation and storage

HNSCC patients undergoing surgery were recruited in accordance with an approved Emory University Institutional Review Board protocol (WINSHIP4008-17), with all patients providing informed consent. All patients had previously untreated locally advanced disease at the time of surgery, presented with a locally metastatic lymph node and were classified as Stage I by the AJCC 8th edition staging guide (Extended Data Table 1). Tumour samples (primary/metastatic) obtained from transoral robotic surgery and/or radical neck dissection were immediately collected and stored in Leibovitz's L-15 medium. Tissue samples were minced into small pieces and digested using an enzymatic cocktail of collagenase I, II, and IV, elastase and DNAse (Worthington) as described previously[33]. Lymphocytes were isolated by using a 44%/67% Percoll gradient. Peripheral blood samples were collected in sodium citrate CPT cell preparation tubes (BD) at time of surgery and processed immediately to obtain peripheral blood mononuclear cells (PBMCs) and plasma. After lysis of red blood cells using ACK Lysing buffer, PBMCs were washed 4 times with Dulbecco's phosphate buffered saline without calcium and magnesium (DPBS) plus 2% fetal calf serum (FCS). Tissue lymphocytes and PBMCs were used fresh for antibody-secreting cell (ASC) ELISPOTs or cryopreserved in 90% FCS with 10% DMSO, and eventually stored in liquid nitrogen. Plasma was stored at −20°C. Healthy control samples were used from healthy individuals, who provided informed consent and were enrolled in several Emory University Institutional Review Board approved protocols studying immune responses to influenza.

Flow cytometry

PBMCs and lymphocytes isolated from tumours were first stained in DPBS containing 2% FCS with Live/Dead Fixable Aqua or Yellow Dead Cell Stain (Invitrogen), followed by addition of antibodies (1 test per 2x10^6 cells; Extended Data Table 2) in BD Horizon Brilliant Stain buffer. Intranuclear staining was performed after fixation and permeabilisation using the Foxp3 Transcription Factor Staining Buffer Set (eBioscience). Samples were acquired with a BD LSRII (FACSDiva v8.0.1) and analysed using FlowJo v9.9.5. Cell sorting was performed using a BD FACSAria II. Cell populations were identified based on the gating strategy outlined in Extended Data Fig. 8.

Antigens

Recombinant HPV antigens fused with maltose-binding protein (MBP) were expressed in *E. coli*. Briefly, DNA sequences encoding HPV16 E2 (Uniprot P03120), HPV16 E6 (Uniprot P03126) and HPV16 E7 (Uniprot P03129) were amplified from a synthetic E2-E6-E7 gene construct (Genscript), equipped with a 3' HisTag-encoding sequence and cloned in-frame into the bacterial expression vector pMAL-c5X (NEB) using NdeI and EcoRI, resulting in fusion proteins with a N-terminal MBP moiety and C-terminal HisTag. MBP with a C-terminal HisTag was generated as a control. Protein expression was performed in NEB

Express competent cells induced overnight at 20°C with IPTG. Soluble MBP-fusion proteins were purified using HisPur Cobalt resin (Thermo) and stored in DPBS with 50% glycerol and 5mM β-ME at −20°C. HPV E2 protein was fluorescently-labelled using the Lightning Link Rapid Alexa Fluor 488 kit (Expedeon). Quadrivalent, inactivated seasonal influenza vaccine Fluarix (GSK) of the 2018/2019 or 2019/2020 season was used to assess influenza-specific responses.

ELISA and ELISPOT

For ELISAs, 100ng of recombinant MBP-fusion protein or MBP alone per well was coated on Nunc Maxisorp ELISA plates overnight at 4°C in 100µl of sodium bicarbonate pH9.6. After coating, unbound protein was removed by washing with DPBS plus 0.05% Tween-20 (DPBS-T) and plates were blocked for 90 min at room temperature with DPBS-T plus 10% FCS (blocking buffer). Plates were washed with DPBS-T and incubated with three-fold serial dilutions of plasma or monoclonal antibodies (mAbs) in blocking buffer for 90 min at room temperature. After washing with DPBS-T, plates were incubated for 90 min with horseradish peroxidase (HRP)-conjugated detection antibodies (1:5000 dilution of anti-human IgG, IgA, IgM; 1:1000 dilution of anti-human IgG1/IgG2/IgG3/IgG4). After washing with DPBS-T and DPBS, plates were developed with the SIGMAFAST OPD tablet set for 5 min (IgG/A/M) or 10 min (IgG1/2/3/4) and stopped by addition of 1M HCl. The optical density (OD) was determined at 490nm. OD of MBP-coated control wells was subtracted from MBP-fusion proteins to account for serum Ig reactivity to MBP. Ig ELISA titres are represented as interpolated plasma dilution required to obtain an OD of 0.5.

For mAb competition ELISAs, MBP-E2 coated plates were incubated with 5µg human mAb per well for 2 hours prior to adding 5ng of mouse IgG2c mAb, an amount resulting in a OD between 1 and 2 in the absence of competing antibody, followed by a 90 min incubation. ELISA was performed as described above using a HRP-conjugated anti-mouse IgG detection antibody (1:2500). Competition is represented as % signal reduction. Binding patterns were clustered using Euclidean distance and average linkage with ClustVis (https://biit.cs.ut.ee/clustvis/).

ELISPOT plates were coated with 1µg of anti-human IgG, 1µg of anti-human IgG/A/M, 1µg MBP-fusion protein, or 0.6µg of Fluarix per well overnight at 4°C to detect total IgG-secreting, total IgA/M or antigen-specific IgG-secreting cells, respectively. After coating, plates were washed with DPBS plus 0.05% Tween-20 (DPBS-T) and DPBS, and blocked for 90 min at 37°C and 5% CO_2 with RPMI supplemented with 1% Penicillin/Streptomycin, L-glutamine, 55µM β-ME and 10% FCS (R10). Three-fold serial dilutions of freshly isolated PBMCs or lymphocytes in R10 were plated and incubated for 6-16 h at 37°C and 5% CO_2. In general, at the lowest dilution 210,000 cells were plated to detect total IgG/A/M- or antigen-specific IgG-secreting ASCs with the exception of 70,000 cells tissue-derived lymphocytes being plated for total IgG/A/M detection, due to the high ASC frequency and to conserve sample material. The number of plated cells was adjusted in case of insufficient cellularity. After washing with DPBS-T and DPBS, plates were incubated with biotinylated anti-human isotype-specific detection antibodies (1:1000) for 2 h. After washing with DPBS-T, plates were incubated with HRP-conjugated avidin D for 1 h. After washing

with DPBS-T and DPBS, plates were developed with 3-Amino-9-ethylcarbazole (AEC) substrate, dried and acquired (Immunospot CTL ELISPOT Reader) followed by manual spot assessment. For memory B cell assays, cryopreserved PBMCs were thawed, resuspended in R10 and stimulated for 4-5 days with 10ng/ml IL-2 (Peprotech) and 1μg/ml R848 (Sigma) at 37°C and 5% CO_2. Stimulated PBMCs were extensively washed and ELISPOT assay was performed for 5 h as described above.

Western blot

10ng of purified MBP-E2 protein per lane was separated in reducing SDS-PAGE followed by transfer to PVDF membranes. After blocking with tris-buffered saline with 0.1% Tween-20 (TBS-T) containing 3% non-fat dry milk (Biorad), membranes were incubated with 1 μg/ml recombinant E2-specific mAbs (hIgG1 backbone) in blocking buffer for 60 min. Membranes were washed with TBS-T and subsequently incubated with a HRP-conjugated anti-human IgG antibody (1:5000) for 60 minutes. After washing with TBS-T and DPBS, bound HRP was detected using the SuperSignal WestPico Chemiluminescent Substrate (Thermo).

HPV genotyping

DNA was isolated from formalin-fixed, paraffin-embedded (FFPE) tissue curls using the QIAamp DNA FFPE Tissue Kit. Initially, DNA integrity was confirmed by amplification of a 408bp β-globin PCR product using the GH20/21 primer set. HPV amplification was performed using a nested PCR approach employing the degenerate MY09/11 and consensus GP5+/GP6+ primers as described previously[34] with minor modifications such as the use of the high-fidelity DNA polymerase Q5 (NEB) and optimized annealing temperatures. PCR products were purified, sequenced and analysed using BLAST (https://blast.ncbi.nlm.nih.gov/Blast.cgi).

mAb generation

Total live ASCs ($CD3/14/16^{-}CD19^{+}CD20^{-}IgD^{-}CD38^{hi}CD71^{+}$) or E2-specific activated B cells ($CD3/14/16^{-}CD19^{+}CD20^{+}IgD^{-}CD71^{+}MBP\text{-}E2^{+}$) were single cell sorted into 96-well plates containing cell lysis buffer. Cloning of IgG heavy and light chain genes was performed as described previously[35] with minor modifications. Analysis of V(D)J usage and somatic hypermutation of cloned mAb sequences was performed using IgBLAST (https://www.ncbi.nlm.nih.gov/igblast/). Recombinant mAbs were produced using the Expi293 expression system (Thermo). The Expi293F cell line was not authenticated after purchase and not tested for mycoplasma contamination. Recombinant mAbs were expressed as human IgG1 as well as mouse IgG2c, in order to enable competition ELISAs. Antibodies were purified from cell culture supernatants using protein A agarose (Genscript).

Multiplex immunohistochemistry and image analysis

7-color multiplex immunohistochemistry was performed with the OPAL Polaris system (Akoya Biosciences). Four to five-micron sections of FFPE tumours from HNSCC patients were deparaffinised, hydrated, and stained manually with anti-CD19 (1:400), anti-CD20 (1:1000), anti-CD138 (1:200), anti-Ki67 (1:200), anti-IRF4 (1:1000), and anti-P16 (1:100)

antibodies (Extended Data Table 2). Heat induced epitope retrieval in EDTA (pH9) or citrate (pH6) buffer was performed prior to blocking non-specific binding and staining the tissues with the primary antibodies. The sections were sequentially stained with each primary, HRP-conjugated secondary antibody, tyramide signal amplification, and OPAL fluorophore according manufacturer's instructions. OPAL 480 (CD19), 520 (IRF4), 570 (Ki67), 620 (P16), 690 (CD20), and 780 (CD138) dyes were used. The sections were counterstained with spectral DAPI (Akoya Biosciences). The stained slides were imaged and scanned using the Vectra Polaris multispectral imaging system.

Random tumor areas (that included tumor parenchyma and stroma) of high-resolution whole slide scanned images were first annotated in PhenoChart 1.0.12 (Akoya Biosciences) and then analyzed with the inForm2.4.8 software (Akoya Biosciences). Tumour parenchyma and stroma areas were identified using DAPI and P16 as a marker for the tumour. For HPV-negative tumors, CD138 was used as a surrogate marker for tumour. Adaptive cell segmentation was accomplished based on nuclear DAPI and membranous CD20. At least 25 cells from the phenotypes of the immune cells of interest were manually selected and used to train the software for automated analysis. Six representative regions per tumour sample were analysed for a total area of 3.8 mm^2 per tumour. The data were processed in R studio using phenoptr (v0.2.5) phenoptrReports (v0.2.6) (Akoya Biosciences).

scRNA-seq analysis

Activated cells of the B cell lineage (live CD3/14/16$^-$CD19$^+$IgD$^-$CD71$^+$) from PBMCs of a healthy donor receiving Fluarix 7 days prior and from lymphocytes from metastatic lymph nodes and primary tumours of 3 HPV+ HNSCC patients were isolated by FACS. Single-cell suspensions of FACS-purified cells were loaded onto the 10X Genomics Chromium Controller. Library construction was performed using the Chromium Single Cell 5' Library Construction Kit followed by sequencing on a HiSeq3000 or NovaSeq6000. Alignment, filtering, barcode counting, and unique molecular identifier counting were performed using Cell Ranger v3.1. Data were further analysed using Seurat v.3.1.4[36]. All single cell analysis was performed using R v.3.6.2. Briefly, cells with a percentage of mitochondrial genes below 0.07% were included. Cells with more than 6000 or fewer than 1000 detected genes were considered as outliers and excluded from the downstream analyses. Samples from different patients were merged using the Seurat function FindIntegrationMarkers, which identifies and calculates anchors between pairs of datasets to reduce the sample batch effect[37]. As immunoglobulin gene transcripts constitute the majority of the transcriptome of the ASC/GC clusters, immunoglobulin genes were excluded from the analysis, unless stated otherwise. Raw unique molecular identifier counts were normalised to unique molecular identifier count per million total counts and log-transformed. Variable genes were selected based on average expression and dispersion. Principal component analysis was performed, and the top 6 most statistically significant principal components were used for UMAP analysis. Clusters and UMAP plots were generated based on principal component analysis dimensions. Marker genes that were differentially expressed within each cluster were identified by the Seurat function FindAllMarkers with average log fold change cutoffs of 0.5. Scaled expression data of the top 10 marker genes were used to create the heatmap. Normalised data are shown in the form of feature plots or violin

plots. Gene set scoring was performed using the VISION R package v.2.1.0, following the scoring algorithm as previously described[38]. Briefly, expression of signature genes is weighted based on predicted dropout probability calculated from nearest neighbors, and the normalised expression summed for all genes in the gene set. ABC and ASC gene sets were derived from Ellebedy et al. 2016[17]. The dark zone GCB signature was derived from Milpied et al. 2018[39], while the proliferation signatures were taken from the Seurat proliferating gene set for S and G2M phases of the cell cycle. Signature scores calculated for each population with the VISION package were transformed into a binary numeric vector and a Pearson's Chi-squared test for binary variables with Yates continuity correction was performed to determine statistical significance. Bonferroni correction for p value adjustments was employed and significance was accepted at $p<0.05$.

Bulk RNA-seq analysis

Naïve B cells (live CD3/14/16$^-$CD19$^+$CD20$^+$IgD$^+$CD27$^-$), antibody-secreting cells (live CD3/14/16$^-$CD19$^+$CD20$^-$IgD$^-$CD38^{hi} CD71$^+$), activated B cells (live CD3/14/16$^-$CD19$^+$CD20$^+$IgD$^-$CD71$^+$CD10$^-$) and germinal centre B cells (live CD3/14/16$^-$CD19$^+$CD20$^+$IgD$^-$CD71$^+$CD10$^+$) were directly sorted into RLT buffer followed by isolation of RNA using the QIAGEN Allprep DNA/RNA Micro Kit. Library preparation and sequencing was performed by the Yerkes Nonhuman Primate Genomics Core at Emory University. RNA-seq analysis was performed as described previously[40]. Briefly, reads were aligned to the human genome (GRCh38; accessed via Ensembl[41]) with HISAT2[42]. Alignments were sorted and indexed with samtools[43], and aligned reads assigned to the Ensembl reference transcriptome release 90 with featureCounts[44]. Normalization for library size, log transformation, and differential expression analysis were performed with DESeq2[45].

Principal component analysis (PCA) was performed with log-transformed data using the FactoMinerR package[46]. *k*-means clustering was performed with the kmeans function in R, and number of clusters was determined by consensus clustering[47]. Data were visualised with ggplot2[48].

Statistical analysis

Data are presented either as mean ± s.e.m. or in case of violin plots median and quartiles are indicated. Friedman test with two-sided Dunn's multiple comparisons test was performed when comparing multiple groups with *p<0.05, **p<0.01, ***p<0.001, and ****p<0.0001. Two-tailed Mann-Whitney was performed to compare HPV-specific IgG antibody titres in p16- and p16+ HNSCC patients with *p<0.05, **p<0.01, ***p<0.001, and ****p<0.0001. Paired two-tailed t-test was used to compare Ki-67 expression of ASCs in PBMCs and tissue with *p<0.05, **p<0.01, ***p<0.001, and ****p<0.0001. For correlative analyses Spearman correlation was performed and r and two-tailed p value being reported. Two-way repeated measures (RM) ANOVA with Sidak's multiple comparisons test was used to compare the distribution of different B cell subsets in the TME with *p<0.05, **p<0.01, ***p<0.001, and ****p<0.0001. All statistical analyses were performed using GraphPad Prism v8.3.

Extended Data

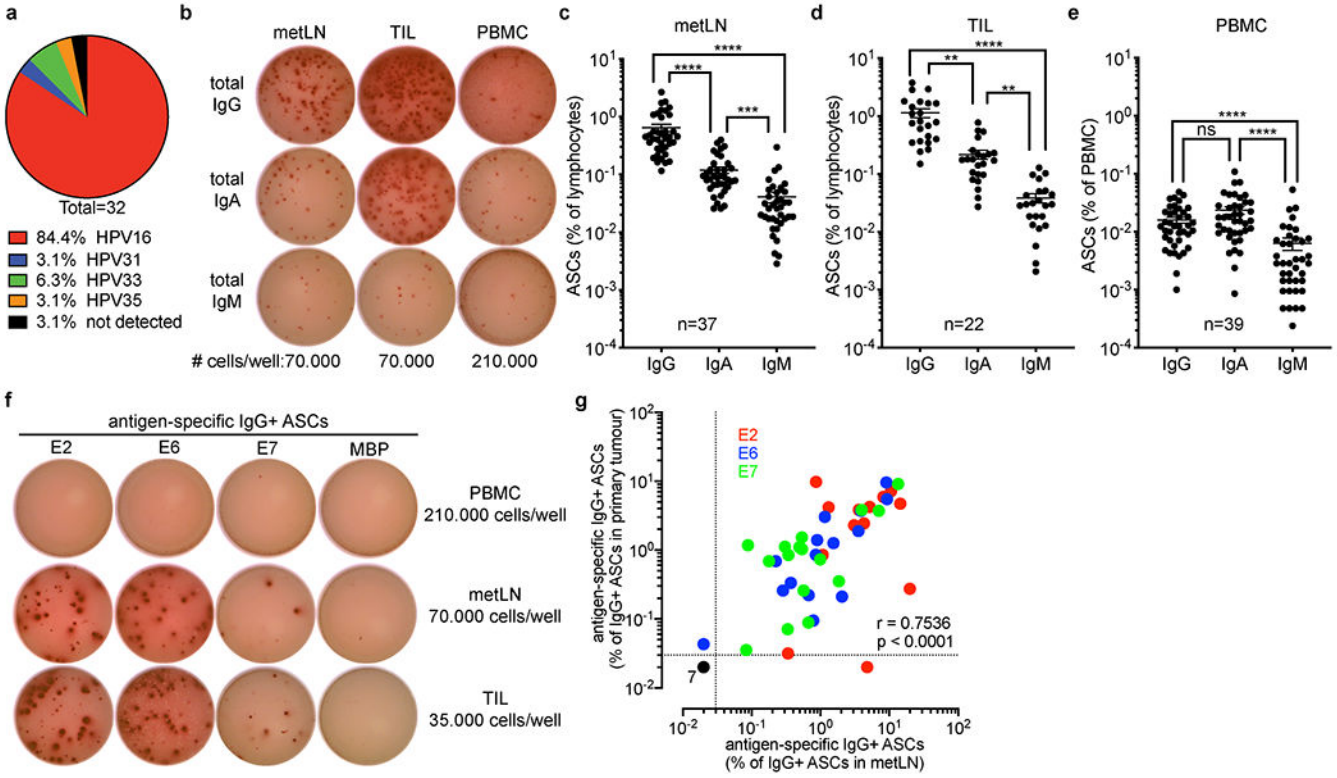

Extended Data Figure 1. HPV-negative HNSCC patients exhibit reduced lymphocyte infiltration into the tumour and lack HPV-specific ASCs.

a, Sequencing-based HPV genotyping of p16+ HNSCC cases (n=32). **b,** Representative ELISPOT showing total antibody-secreting cells (ASCs) among lymphocytes from metastatic lymph node (metLN), primary tumour (TIL) and PBMC of a p16+ HNSCC patient. **c-e,** Summary graphs showing the frequency of ASCs producing IgG, IgA and IgM among lymphocytes from metLN (n=37) **(c)**, TIL (n=22) **(d)** or PBMC (n=39) of p16+ HNSCC patients **(e)**. Results with mean ± s.e.m. are shown. Friedman test with two-sided Dunn's multiple comparisons test was performed for data in **c-e**. **(c)** ***p=0.0001, ****p<0.0001; **(d)** **p=0.0021, ****p<0.0001; **(e)** ****p<0.0001, ns=0.1720. **f,** Representative ELISPOT of E2/6/7-specific IgG-secreting ASCs in PBMC, metLN and TIL of a p16+ HNSCC patient. MBP (maltose-binding protein) indicates negative control. **g,** Correlation (Spearman) of antigen-specific IgG-secreting ASCs in metLN and TIL (n=18 patients) with r=0.7536 and p<0.0001.

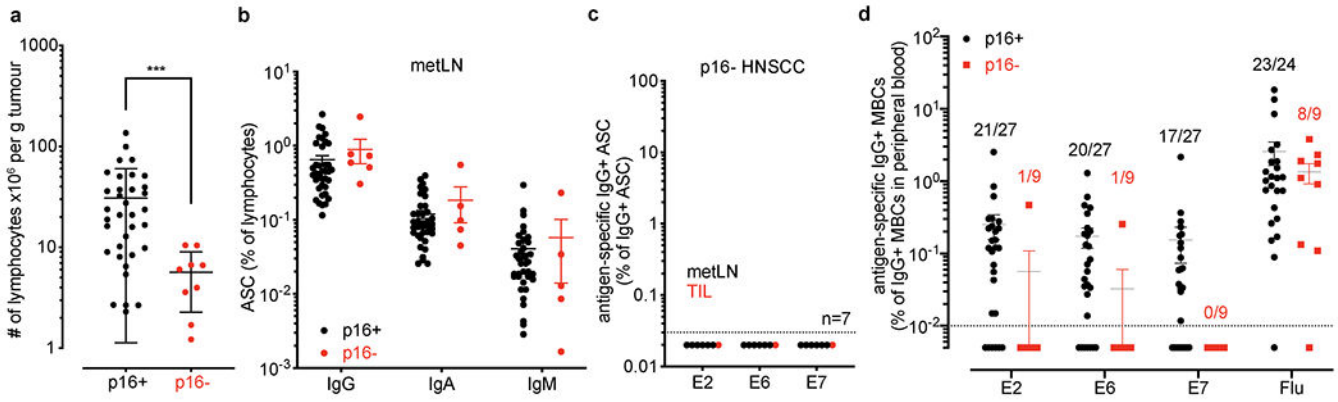

Extended Data Figure 2. HPV-negative HNSCC patients exhibit reduced lymphocyte infiltration into the tumour and lack HPV-specific ASCs.

a, Number of isolated lymphocytes per gram primary tumour in p16+ (n=35) and p16- (n=9) HNSCC patients. Two-tailed Mann-Whitney with ***p=0.0007. **b,** Frequency of ASCs producing IgG, IgA and IgM among lymphocytes from metLN of p16+ (n=37) and p16- (n=6 for IgG, n=5 for IgA and IgM) HNSCC patients. **c,** Frequency of E2/6/7-specific IgG-secreting ASCs among total IgG-secreting ASCs in metLN (n=6) and TIL (n=1) of p16- HNSCC patients. **d,** Frequency of E2/6/7- and Influenza (Flu)-specific IgG+ memory B cells (MBCs) among total IgG+ MBCs in the peripheral blood of p16+ (n=27) and p16- (n=9) HNSCC patients. Numbers indicate detected responses among tested samples. Results with mean ± s.e.m. are shown.

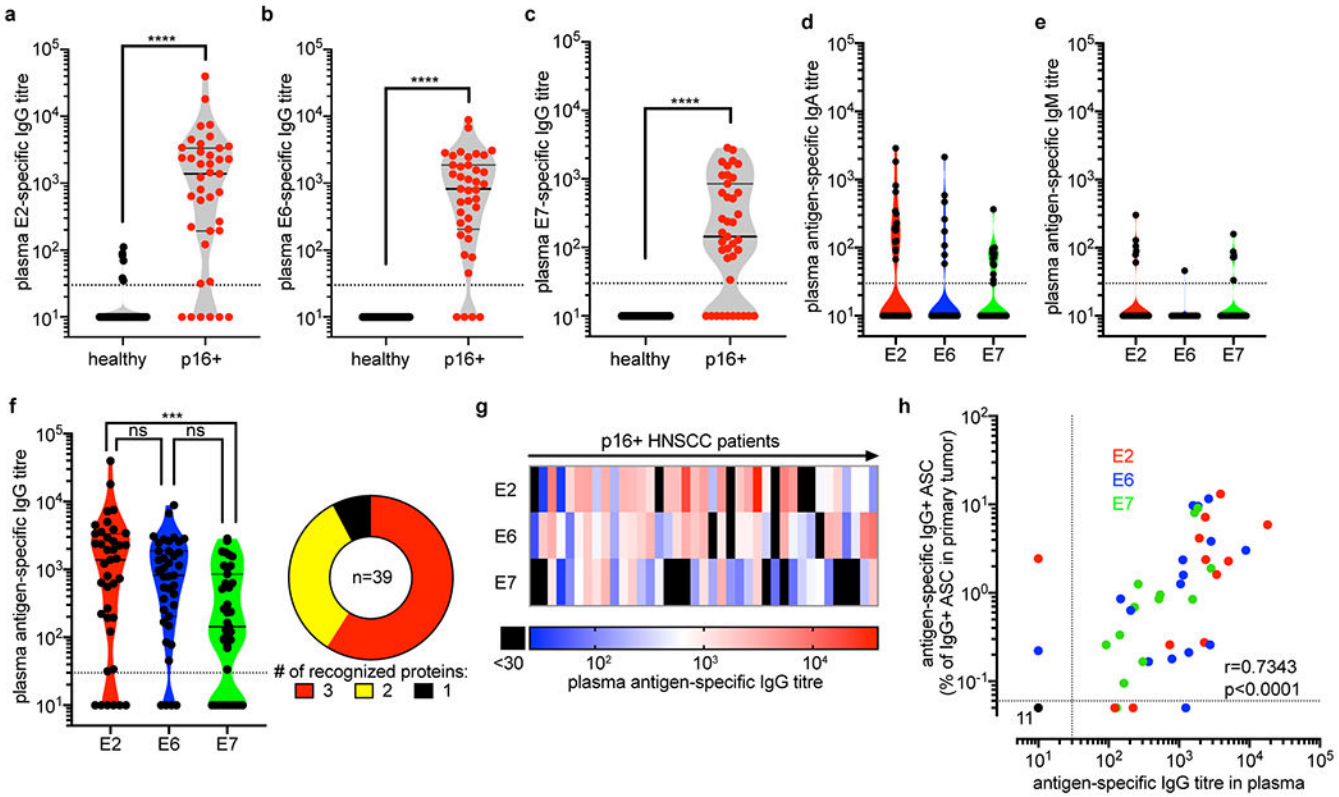

Extended Data Figure 3. Serological analyses.

a-c, IgG titres against E2 **(a)**, E6 **(b)**, and E7 **(c)** in plasma of healthy individuals (n=50) and p16+ HNSCC patients (n=39). Results with median and quartiles are shown. Two-tailed Mann-Whitney with ****p<0.0001. **d,e,** E2/6/7-specific IgA **(d)** and IgM **(e)** titres in plasma of p16+ patients (n=39). **f,** E2/6/7-specific IgG titres in plasma of p16+ patients and graph demonstrating an IgG response against at least 2 HPV proteins in the vast majority of patients (n=39). Results with median and quartiles are shown. Friedman test with two-sided Dunn's multiple comparisons test with ***p=0.0006, ns=0.1852. **g,** Heatmap showing E2/6/7-specific IgG antibody titres in p16+ HNSCC patients (n=39) with each column representing a patient. **h,** Correlation (Spearman) between E2/6/7-specific IgG+ ASCs in primary tumour and E2/6/7-specific IgG titres in plasma (n=18 patients) with r=0.7343 and p<0.0001.

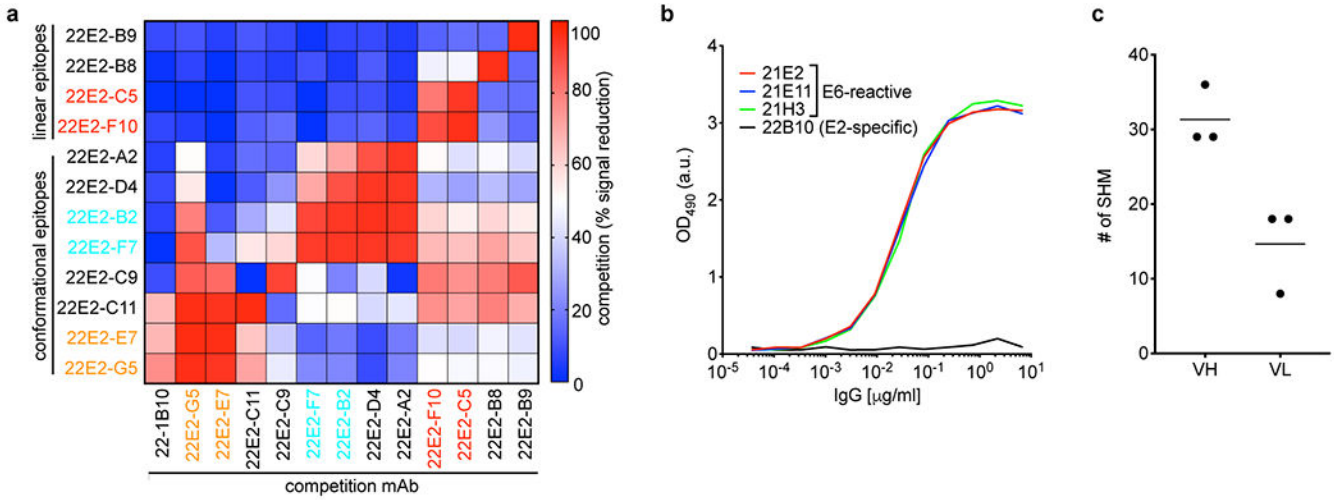

Extended Data Figure 4. Human monoclonal antibodies against HPV E antigens.

a, Clustered binding pattern of E2-specific mAbs performed by competition ELISA. Recognition of linear epitopes was determined by Western blot. **b,** ELISA of E6-specific mAbs (21E2, 21E11, 21H3) generated from single cell sorted ASCs from metLN of a HPV+ HNSCC patient. An E2-specific mAb (22B10) is shown as negative control. arbitrary units (a.u.). **c,** Number of somatic hypermutations (SHM) in the VH and VL chain of E6-specific mAbs (n=3) with indicated mean.

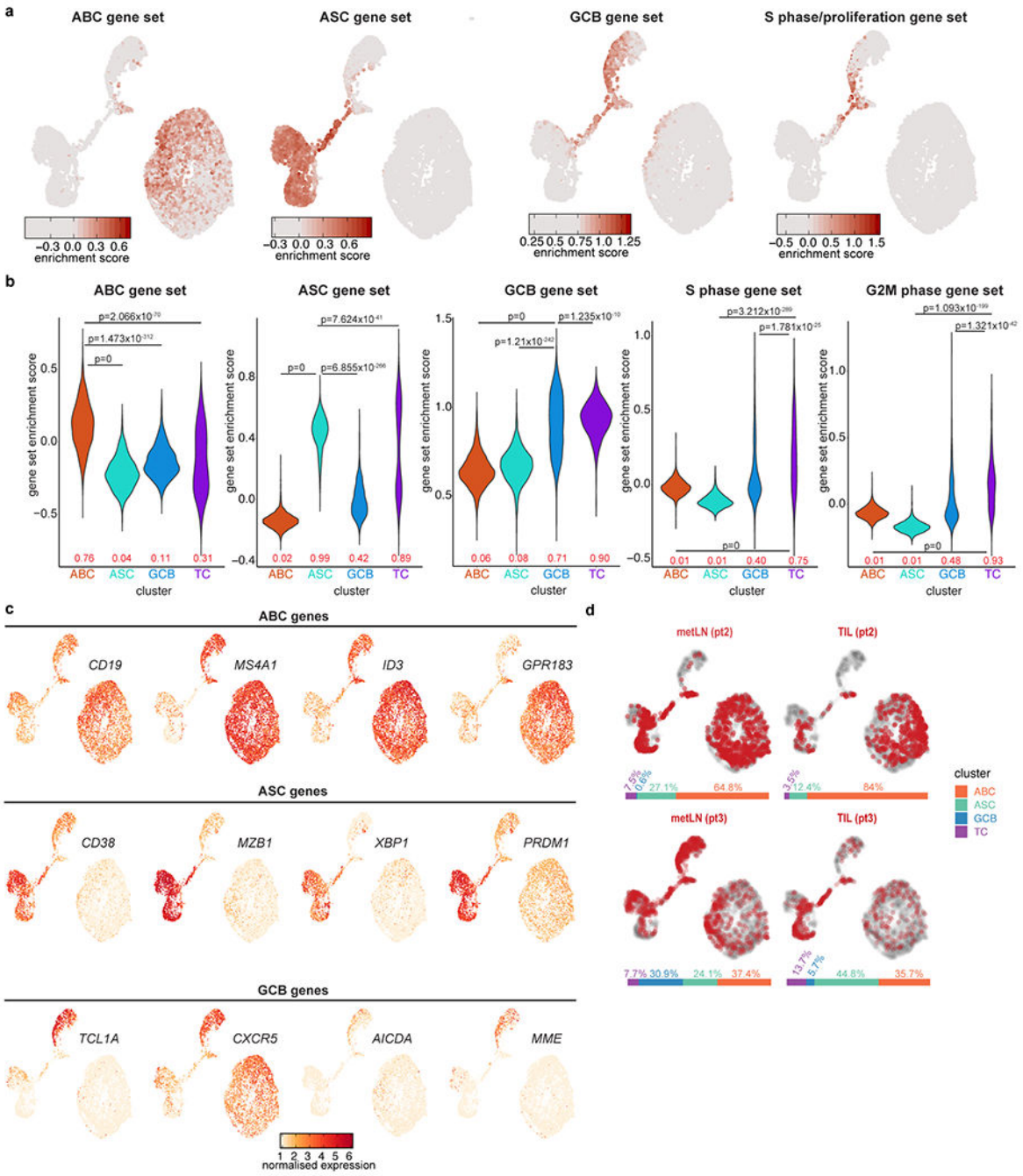

Extended Data Figure 5. Activated cells of the B cell lineage from the tumour microenvironment are present in distinct clusters.

a, UMAP plots showing enrichment for activated B cell (ABC), antibody-secreting cell (ASC), germinal centre B cells (GCB) and proliferation gene sets. **b,** Violin plots showing gene set enrichment scores among the 4 clusters identified by scRNAseq. Two-sided Pearson's Chi-squared test for binary variables with Yates continuity correction was performed (sample estimates in red). p values are indicated for select comparisons. **c,** UMAP plots showing expression of selected genes. **d,** UMAP plots showing distribution of cells

of the indicated patient and tissue origin (in red) among the identified clusters. Bar graphs quantifying the composition of the respective sample in terms of frequency among the identified clusters: antibody-secreting cells (ASC), activated B cells (ABC), germinal centre B cells (GCB), and transitory cells (TC).

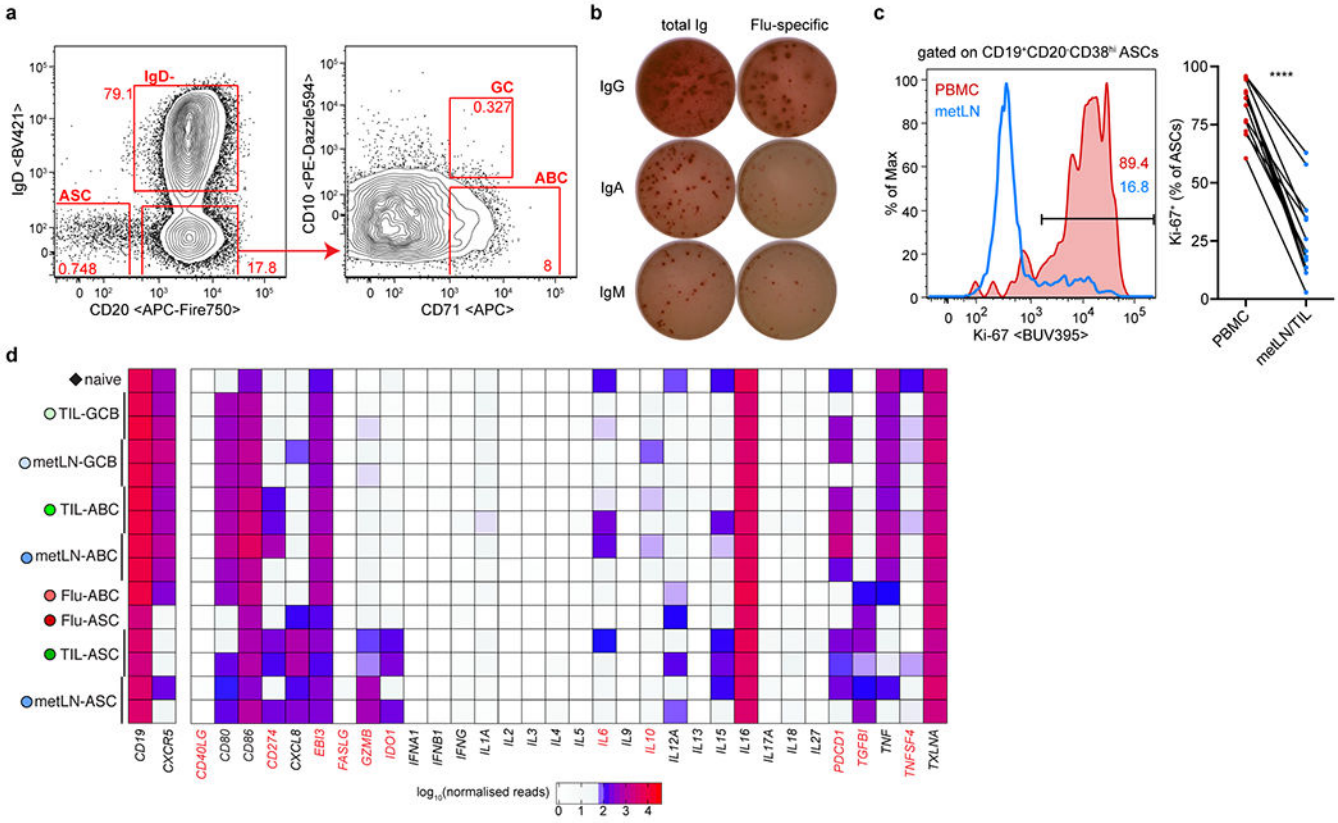

Extended Data Figure 6. Gene expression of cytokines and other immunomodulators by B cells and plasma cells in the TME.

a, Flow plots showing the presence of ASCs and ABCs but absence of germinal centre (GC) B cells in the peripheral blood of a healthy volunteer 7 days post vaccination with Fluarix. **b,** ASC ELISPOT showing total IgG/A/M-secreting cells (upper panel) and influenza (Flu)-specific IgG/A/M-secreting cells (lower panel) in PBMCs 7 days post vaccination with Fluarix. **c,** Representative histogram of ASCs from peripheral blood (red) or metLN (blue) of HNSCC patients showing Ki-67 expression. Numbers indicate frequency of Ki-67+ cells among total ASCs. Summary graph showing paired frequencies of Ki-67-expressing ASCs in PBMCs and metLN/TIL (n=14). Paired two-tailed t-test with ****p<0.0001. **d,** Heatmap showing gene expression (normalised reads) of selected cytokines and immunomodulators as well as CD19 and CXCR5 as reference. Immunomodulators related to B cells and previously described as negative regulators in the TME are highlighted in red. An expression threshold was set to 50 normalised reads, with reads <50 displayed in white.

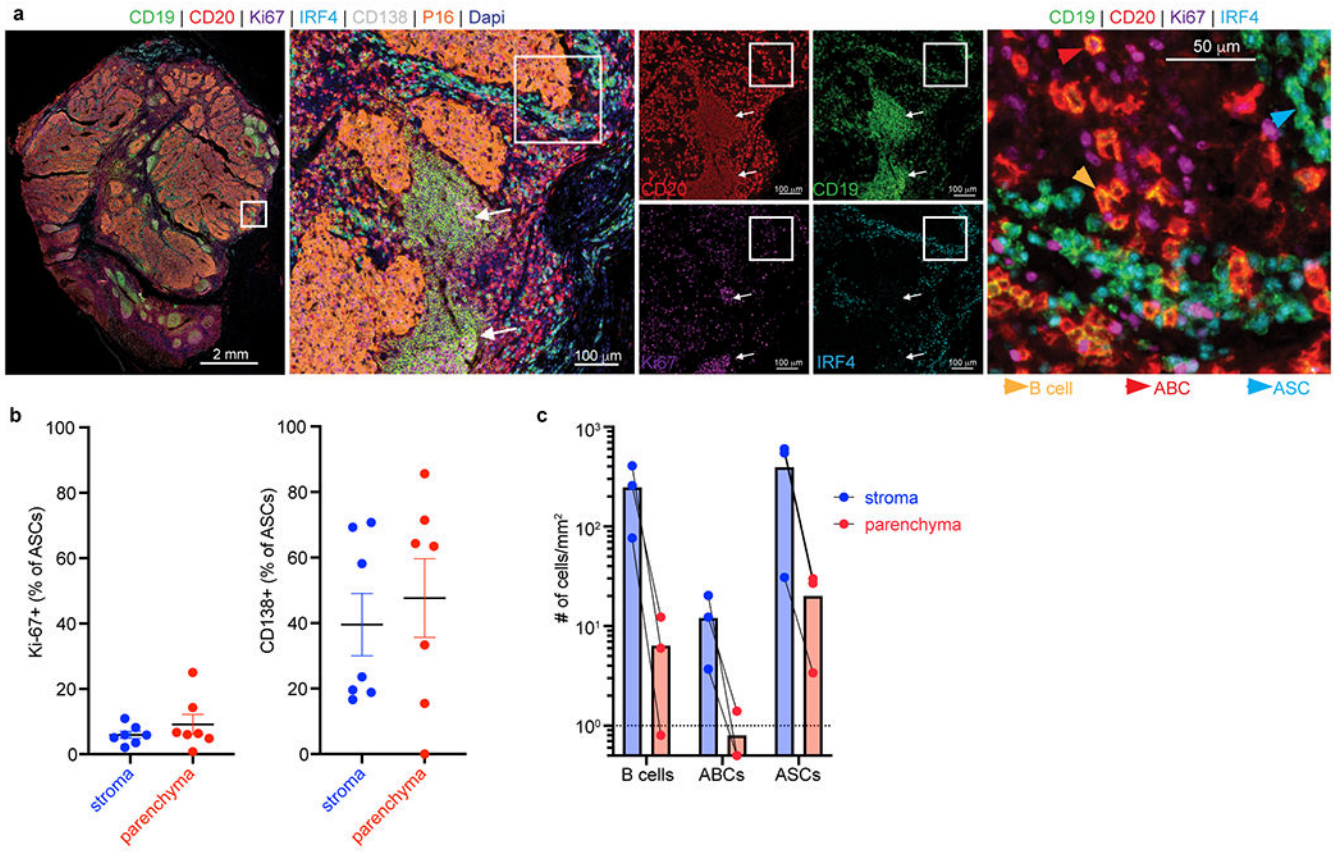

Extended Data Figure 7. mIHC analysis of B cells and ASCs in the TME.

a, Representative mIHC section of HPV+ HNSCC tumour (n=7) with B cell infiltrates and associated germinal centres (white arrows) (see also main Fig.5e). 7-colour composite mIHC images of CD19, CD20, Ki-67, IRF4, CD138, P16, and DAPI (left panels), individual images of CD20, CD19, Ki-67, and IRF4 (middle panels), and high magnification (right panel) of a region of interest (white box). **b,** Frequency of Ki-67+ and CD138+ ASCs (CD19+CD20-IRF4+) in mIHC sections of 7 HPV+ HNSCC tumours. Results with mean ± s.e.m. are shown. **c,** Quantification of B cells (CD19+CD20+), ABCs (CD19+CD20+Ki-67+), and ASCs (CD19+CD20-IRF4+) in the stroma and tumour parenchyma of 3 HPV- HNSCC patients.

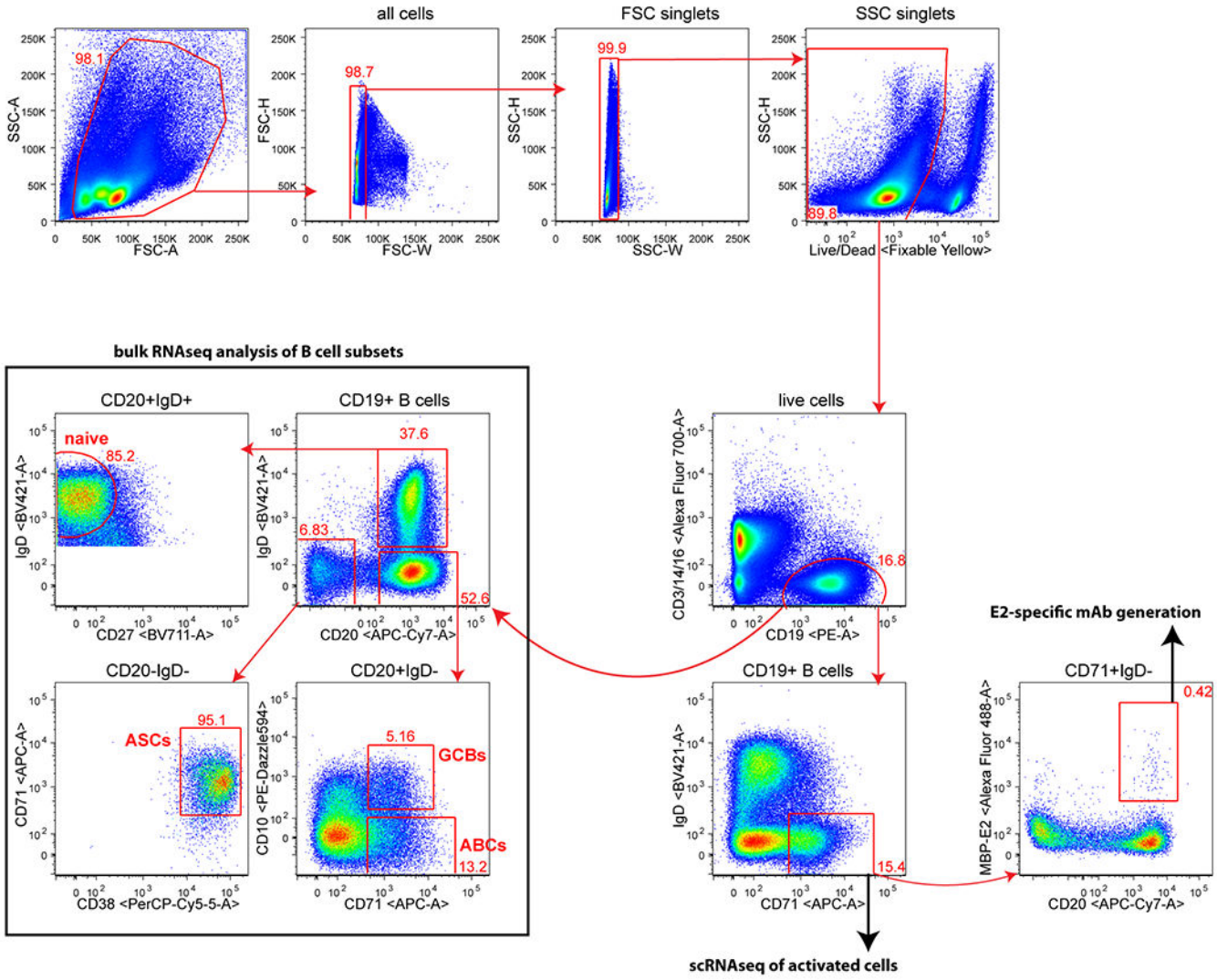

Extended Data Figure 8. Gating strategy for isolation/analysis of B cell subsets.

Gating strategy for B cell subsets used for flow cytometric analyses, bulk RNAseq analyses, scRNAseq analyses, or the generation of E2-specific monoclonal antibodies (mAbs). B cell subsets used for bulk RNAseq analyses are highlighted in red: antibody-secreting cells (ASCs), activated B cells (ABCs), germinal centre B cells (GCBs).

Extended Data Table 1
Patient characteristics.

Pathological features include lymphovascular invasion (LVI), perineural invasion (PNI), and extranodal extension (ENE).

Demographic	n = 43
Male	36 (84 %)
Female	7 (16%)
Average Age	57 (Range 44 - 75)

Demographic	n = 43
Tobacco Exposure	
0 years	29 (67 %)
< 10 years	5 (12 %)
≥ 10 years	9 (21 %)
Tumour Subsite	
Tonsil	30 (70 %)
Base of Tongue	11 (25 %)
Unknown	2 (5 %)
Stage 8th AJCC	
T0	2 (5 %)
T1	16 (37 %)
T2	23 (53 %)
T3	2 (5 %)
N0	3 (7 %)
N1	37 (86 %)
N2	3 (7 %)
M0	43 (100 %)
Pathology Features	
Margins	
positive	1 (2 %)
negative	42 (98 %)
LVI	22 (51 %)
PNI	9 (21 %)
ENE	16 (37 %)
Node Count	31 (Range 10-71)
# Positive Nodes	
0	3 (7%)
1	25 (58 %)
2	11 (25 %)
3	2 (5 %)
4	1 (2 %)
>4	1 (2 %)

Extended Data Table 2

List of antibodies and reagents.

Reagent	Source	Identifier
Antibodies for flow cytometry		
anti-CD10	Biolegend	clone: HI10a; RRID: AB_2565878

Reagent	Source	Identifier
anti-CD14	Biolegend	clone: M5E2; RRID: AB_493747
anti-CD16	Biolegend	clone: 3G8; RRID: AB_2278418
anti-CD19	Biolegend	clone: HIB19; RRID: AB_314238, AB_2562015
anti-CD20	Biolegend	clone: 2H7; RRID: AB_2572126
anti-CD27	Biolegend	clone: 0323; RRID: AB_2563809
anti-CD3	Biolegend	clone: SK7; RRID: AB_2563420
anti-CD38	Biolegend	clone: HIT2; RRID: AB_2565893
anti-CD71	Biolegend	clone: CY1G4; RRID: AB_10915138
anti-IgD	Biolegend	clone: IA6-2; RRID: AB_2561619
anti-Ki-67	BD	clone: B56; RRID: AB_647087, AB_2738577
Antibodies/reagents for ELISPOT and ELISA		
anti-human IgG (coating)	JacksonlmmunoResearch	polyclonal; RRID: AB_2337550
anti-human IgG/A/M (coating)	JacksonlmmunoResearch	polyclonal; RRID: AB_2337538
biotinylated anti-human IgG	JacksonlmmunoResearch	polyclonal; RRID: AB_2340506
biotinyiated anti-human IgA	JacksonlmmunoResearch	polyclonal; RRID: AB_2337624
biotinylated anti-human IgM	Invitrogen	polyclonal; RRID: AB_2536559
HRP-conjugated Avidin D	Vector Laboratories	RRID: AB_2336507
HRP-conjugated anti-human IgG	JacksonlmmunoResearch	polyclonal; RRID: AB_2337586
HRP-conjugated anti-human IgA	JacksonImmunoResearch	polyclonal; RRID: AB_2337592
HRP-conjugated anti-human IgM	JacksonImmunoResearch	polyclonal; RRID: AB_2337598
HRP-conjugated anti-human IgG1	Southern Biotech	clone: HP6001; RRID: AB_2796627
HRP-conjugated anti-human IgG2	Southern Biotech	clone: 31-7-4; RRID: AB_2796633
HRP-conjugated anti-human IgG3	Southern Biotech	clone: HP6050; RRID: AB_2796699
HRP-conjugated anti-human IgG4	Southern Biotech	clone: HP6025; RRID: AB_2796691
HRP-conjugated anti-mouse IgG	Southern Biotech	polyclonal; RRID: AB_2619742
Antibodies for IHC		
anti-Ki67	BD Biosciences	clone: B56; RRID: AB_396287
anti-p16	Enzo	# ENZ-ABS377
anti-CD19	Cell Signaling Technologies	clone: D4V4B; RRID: AB_2800152
anti-IRF4	Agilent	clone: MUM1p; RRID: AB_2127157
anti-CD20	Invitrogen	clone: L26; RRID: AB_10983209
anti-CD138	Biolegend	clone: MI15; RRID: AB_2561790

Supplementary Material

Refer to Web version on PubMed Central for supplementary material.

Acknowledgments

This work was supported by funding from the Ambrose Monell Foundation (R.A.), a Winship Invest$ Pilot grant (to R.A., Z.G.C, and N.F.S.), and NCI grant 1-R00-CA197891 (H.T.K). W.H.H. is a Cancer Research Institute Irvington Fellow supported by the Cancer Research Institute. We would like to acknowledge the pathology personnel involved in sample handling, the Emory Flow Cytometry Core supported by the National Center for Georgia Clinical & Translational Science Alliance of the NIH under award number UL1TR002378, and the Yerkes NHP Genomics Core which is supported in part by NIH P51 OD011132. We would also like to thank Carl W. Davis and Lisa J. Sudmeier for feedback on the manuscript.

Data availability

The following protein sequences were employed for generating recombinant HPV proteins: E2 (Uniprot P03120), E6 (Uniprot03126), and E7 (Uniprot P03129). RNA-seq and scRNA-seq data are available in the NCBI Gene Expression Omnibus (GEO) database under the SuperSeries accession numbers GSE149327 and GSE153559, respectively. Normalised gene expression counts of sorted B cell subsets are available in Supplementary Table 1. Other relevant data are available from the corresponding authors upon reasonable request.

REFERENCES

1. Cabrita R et al. Tertiary lymphoid structures improve immunotherapy and survival in melanoma. Nature 577, 561–565, doi:10.1038/s41586-019-1914-8 (2020). [PubMed: 31942071]
2. Helmink BA et al. B cells and tertiary lymphoid structures promote immunotherapy response. Nature 577, 549–555, doi:10.1038/s41586-019-1922-8 (2020). [PubMed: 31942075]
3. Petitprez F et al. B cells are associated with survival and immunotherapy response in sarcoma. Nature 577, 556–560, doi:10.1038/s41586-019-1906-8 (2020). [PubMed: 31942077]
4. Flynn NJ, Somasundaram R, Arnold KM & Sims-Mourtada J The Multifaceted Roles of B Cells in Solid Tumors: Emerging Treatment Opportunities. Target. Oncol 12, 139–152, doi:10.1007/s11523-017-0481-x (2017). [PubMed: 28281220]
5. Yuen GJ, Demissie E & Pillai S B lymphocytes and cancer: a love-hate relationship. Trends Cancer 2, 747–757, doi:10.1016/j.trecan.2016.10.010 (2016). [PubMed: 28626801]
6. Shalapour S et al. Immunosuppressive plasma cells impede T-cell-dependent immunogenic chemotherapy. Nature 521, 94–98, doi:10.1038/nature14395 (2015). [PubMed: 25924065]
7. Kroeger DR, Milne K & Nelson BH Tumor-Infiltrating Plasma Cells Are Associated with Tertiary Lymphoid Structures, Cytolytic T-Cell Responses, and Superior Prognosis in Ovarian Cancer. Clin. Cancer Res 22, 3005–3015, doi:10.1158/1078-0432.CCR-15-2762 (2016). [PubMed: 26763251]
8. Lechner A et al. Tumor-associated B cells and humoral immune response in head and neck squamous cell carcinoma. Oncoimmunology 8, 1535293, doi:10.1080/2162402X.2018.1535293 (2019). [PubMed: 30723574]
9. Ang KK et al. Human papillomavirus and survival of patients with oropharyngeal cancer. N. Engl. J. Med 363, 24–35, doi:10.1056/NEJMoa0912217 (2010). [PubMed: 20530316]
10. Nulton TJ, Olex AL, Dozmorov M, Morgan IM & Windle B Analysis of The Cancer Genome Atlas sequencing data reveals novel properties of the human papillomavirus 16 genome in head and neck squamous cell carcinoma. Oncotarget 8, 17684–17699, doi:10.18632/oncotarget.15179 (2017). [PubMed: 28187443]
11. Marur S, D'Souza G, Westra WH & Forastiere AA HPV-associated head and neck cancer: a virus-related cancer epidemic. Lancet Oncol. 11, 781–789, doi:10.1016/S1470-2045(10)70017-6 (2010).å [PubMed: 20451455]
12. Mei HE et al. Blood-borne human plasma cells in steady state are derived from mucosal immune responses. Blood 113, 2461–2469, doi:10.1182/blood-2008-04-153544 (2009). [PubMed: 18987362]

13. Ward MJ et al. Tumour-infiltrating lymphocytes predict for outcome in HPV-positive oropharyngeal cancer. Br. J. Cancer 110, 489–500, doi:10.1038/bjc.2013.639 (2014). [PubMed: 24169344]
14. Lang Kuhs KA et al. Characterization of human papillomavirus antibodies in individuals with head and neck cancer. Cancer Epidemiol. 42, 46–52, doi:10.1016/j.canep.2016.03.003 (2016). [PubMed: 27010729]
15. Lang Kuhs KA et al. Human papillomavirus 16 E6 antibodies are sensitive for human papillomavirus-driven oropharyngeal cancer and are associated with recurrence. Cancer 123, 4382–4390, doi:10.1002/cncr.30966 (2017). [PubMed: 28950407]
16. Dahlstrom KR et al. Diagnostic accuracy of serum antibodies to human papillomavirus type 16 early antigens in the detection of human papillomavirus-related oropharyngeal cancer. Cancer 123, 4886–4894, doi:10.1002/cncr.30955 (2017). [PubMed: 28898394]
17. Ellebedy AH et al. Defining antigen-specific plasmablast and memory B cell subsets in human blood after viral infection or vaccination. Nat. Immunol 17, 1226–1234, doi:10.1038/ni.3533 (2016). [PubMed: 27525369]
18. Davis CW et al. Longitudinal Analysis of the Human B Cell Response to Ebola Virus Infection. Cell 177, 1566–1582 e1517, doi:10.1016/j.cell.2019.04.036 (2019). [PubMed: 31104840]
19. Sullivan NL et al. Breadth and Functionality of Varicella-Zoster Virus Glycoprotein-Specific Antibodies Identified after Zostavax Vaccination in Humans. J. Virol 92, doi:10.1128/JVI.00269-18 (2018).
20. Li GM et al. Pandemic H1N1 influenza vaccine induces a recall response in humans that favors broadly cross-reactive memory B cells. Proc. Natl. Acad. Sci. U. S. A 109, 9047–9052, doi:10.1073/pnas.1118979109 (2012). [PubMed: 22615367]
21. Scheid JF et al. Broad diversity of neutralizing antibodies isolated from memory B cells in HIV-infected individuals. Nature 458, 636–640, doi:10.1038/nature07930 (2009). [PubMed: 19287373]
22. Pereira JP, Kelly LM, Xu Y & Cyster JG EBI2 mediates B cell segregation between the outer and centre follicle. Nature 460, 1122–1126, doi:10.1038/nature08226 (2009). [PubMed: 19597478]
23. Barrena S et al. Aberrant expression of tetraspanin molecules in B-cell chronic lymphoproliferative disorders and its correlation with normal B-cell maturation. Leukemia 19, 1376–1383, doi:10.1038/sj.leu.2403822 (2005). [PubMed: 15931266]
24. Arce S et al. CD38 low IgG-secreting cells are precursors of various CD38 high-expressing plasma cell populations. J. Leukoc. Biol 75, 1022–1028, doi:10.1189/jlb.0603279 (2004). [PubMed: 15020647]
25. Green JA et al. The sphingosine 1-phosphate receptor S1P(2) maintains the homeostasis of germinal center B cells and promotes niche confinement. Nat. Immunol 12, 672–680, doi:10.1038/ni.2047 (2011). [PubMed: 21642988]
26. Sharonov GV, Serebrovskaya EO, Yuzhakova DV, Britanova OV & Chudakov DM B cells, plasma cells and antibody repertoires in the tumour microenvironment. Nat. Rev. Immunol, doi:10.1038/s41577-019-0257-x (2020).
27. Sautes-Fridman C, Petitprez F, Calderaro J & Fridman WH Tertiary lymphoid structures in the era of cancer immunotherapy. Nat. Rev. Cancer 19, 307–325, doi:10.1038/s41568-019-0144-6 (2019). [PubMed: 31092904]
28. Skeate JG, Woodham AW, Einstein MH, Da Silva DM & Kast WM Current therapeutic vaccination and immunotherapy strategies for HPV-related diseases. Hum. Vaccin. Immunother 12, 1418–1429, doi:10.1080/21645515.2015.1136039 (2016). [PubMed: 26835746]
29. Chaturvedi AK et al. Human papillomavirus and rising oropharyngeal cancer incidence in the United States. J. Clin. Oncol 29, 4294–4301, doi:10.1200/JCO.2011.36.4596 (2011). [PubMed: 21969503]
30. Krishna S et al. Human Papilloma Virus Specific Immunogenicity and Dysfunction of CD8(+) T Cells in Head and Neck Cancer. Cancer Res. 78, 6159–6170, doi:10.1158/0008-5472.CAN-18-0163 (2018). [PubMed: 30154146]
31. Dahlstrom KR et al. HPV Serum Antibodies as Predictors of Survival and Disease Progression in Patients with HPV-Positive Squamous Cell Carcinoma of the Oropharynx. Clin. Cancer Res 21, 2861–2869, doi:10.1158/1078-0432.CCR-14-3323 (2015). [PubMed: 26078432]

32. Wieland A & Ahmed R Fc Receptors in Antimicrobial Protection. Curr. Top. Microbiol. Immunol, doi:10.1007/82_2019_154 (2019).

Additional references for methods section

33. Kamphorst AO et al. Rescue of exhausted CD8 T cells by PD-1-targeted therapies is CD28-dependent. Science 355, 1423–1427, doi:10.1126/science.aaf0683 (2017). [PubMed: 28280249]
34. de Leon DC et al. Human papillomavirus (HPV) in breast tumors: prevalence in a group of Mexican patients. BMC Cancer 9, 26, doi:10.1186/1471-2407-9-26 (2009). [PubMed: 19161629]
35. Smith K et al. Rapid generation of fully human monoclonal antibodies specific to a vaccinating antigen. Nat. Protoc 4, 372–384, doi:10.1038/nprot.2009.3 (2009). [PubMed: 19247287]
36. Satija R, Farrell JA, Gennert D, Schier AF & Regev A Spatial reconstruction of single-cell gene expression data. Nat. Biotechnol 33, 495–502, doi:10.1038/nbt.3192 (2015). [PubMed: 25867923]
37. Stuart T et al. Comprehensive Integration of Single-Cell Data. Cell 177, 1888–1902 e1821, doi:10.1016/j.cell.2019.05.031 (2019). [PubMed: 31178118]
38. DeTomaso D & Yosef N FastProject: a tool for low-dimensional analysis of single-cell RNA-Seq data. BMC Bioinformatics 17, 315, doi:10.1186/s12859-016-1176-5 (2016). [PubMed: 27553427]
39. Milpied P et al. Human germinal center transcriptional programs are de-synchronized in B cell lymphoma. Nat. Immunol 19, 1013–1024, doi:10.1038/s41590-018-0181-4 (2018). [PubMed: 30104629]
40. Hudson WH et al. Expression of novel long noncoding RNAs defines virus-specific effector and memory CD8(+) T cells. Nat Commun 10, 196, doi:10.1038/s41467-018-07956-7 (2019). [PubMed: 30643116]
41. Zerbino DR et al. Ensembl 2018. Nucleic Acids Research 46, D754–D761, doi:10.1093/nar/gkx1098 (2017).
42. Kim D, Langmead B & Salzberg SL HISAT: a fast spliced aligner with low memory requirements. Nature Methods 12, 357–360, doi:10.1038/nmeth.3317 (2015). [PubMed: 25751142]
43. Li H et al. The Sequence Alignment/Map format and SAMtools. Bioinformatics 25, 2078–2079, doi:10.1093/bioinformatics/btp352 (2009). [PubMed: 19505943]
44. Liao Y, Smyth GK & Shi W featureCounts: an efficient general purpose program for assigning sequence reads to genomic features. Bioinformatics 30, 923–930, doi:10.1093/bioinformatics/btt656 (2013). [PubMed: 24227677]
45. Love MI, Huber W & Anders S Moderated estimation of fold change and dispersion for RNA-seq data with DESeq2. Genome Biology 15, doi:10.1186/s13059-014-0550-8 (2014).
46. Lê S, Josse J & Husson F FactoMineR: AnRPackage for Multivariate Analysis. Journal of Statistical Software 25, doi:10.18637/jss.v025.i01 (2008).
47. Wilkerson MD & Hayes DN ConsensusClusterPlus: a class discovery tool with confidence assessments and item tracking. Bioinformatics 26, 1572–1573, doi:10.1093/bioinformatics/btq170 (2010). [PubMed: 20427518]
48. Wickham H, doi:10.1007/978-0-387-98141-3 (2009).

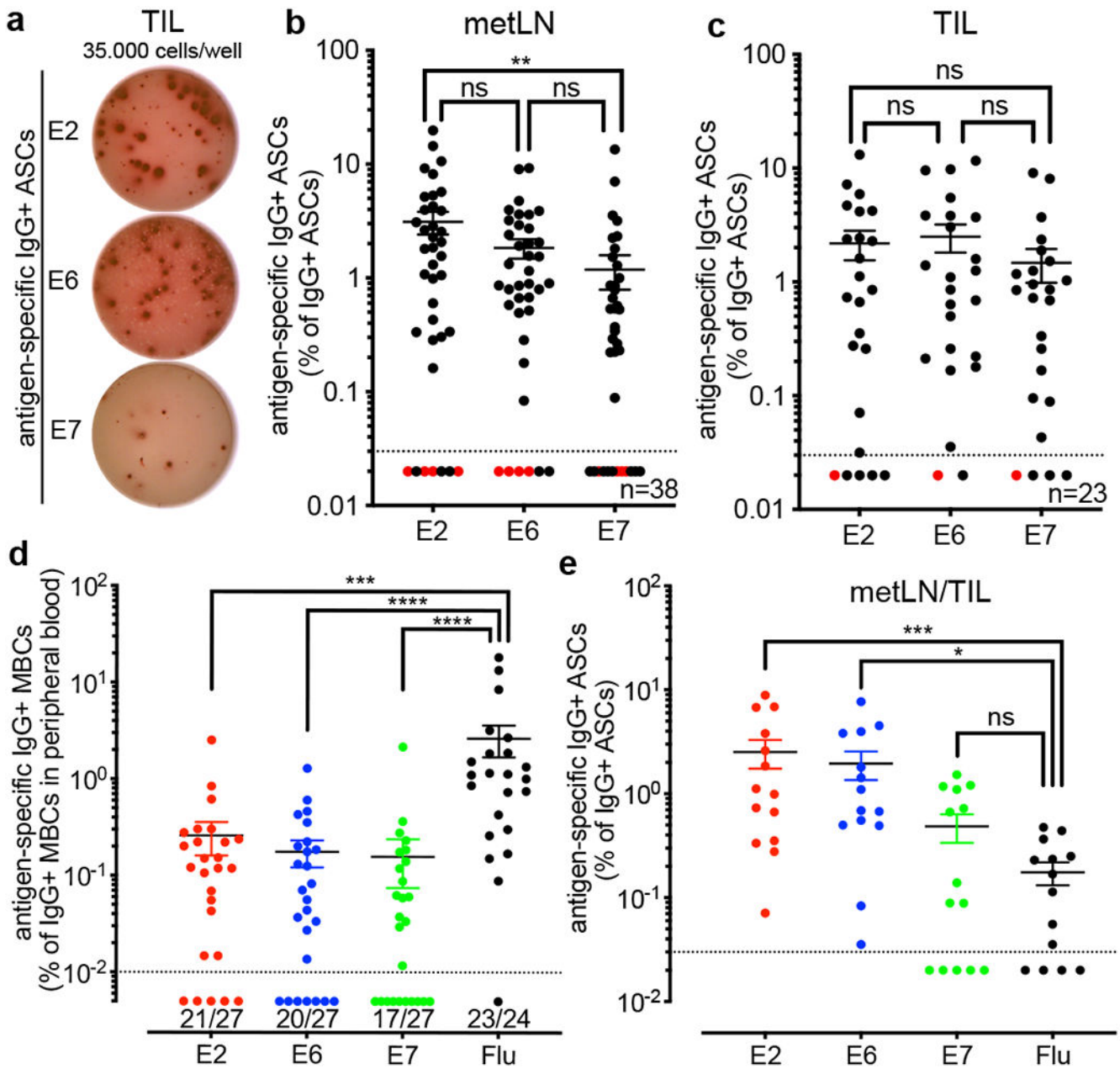

Figure 1. HPV-specific antibody-secreting cells are present in the TME of HPV-positive HNSCC patients.

a, ELISPOT showing E2/6/7-specific IgG-secreting ASCs in tumour (TIL). **b, c,** Frequency of E2/6/7-specific IgG-secreting ASCs among total IgG-secreting ASCs in metastatic lymph node (metLN; n=38) **(b)** and TIL (n=23) **(c)**. Patients without any responses in red. **d,** Frequency of E2/6/7- (n=27) and Influenza (Flu)-specific (n=24) IgG+ memory B cells (MBCs) among total IgG+ MBCs in blood. **e,** Frequency of E2/6/7- and Influenza (Flu)-specific IgG+ ASCs among total IgG+ ASCs in metLN/TIL (n=14). Results with mean ± s.e.m. Friedman test with two-sided Dunn's multiple comparisons test with *p<0.05, **p<0.01, ***p<0.001, ****p<0.0001, ns not significant.

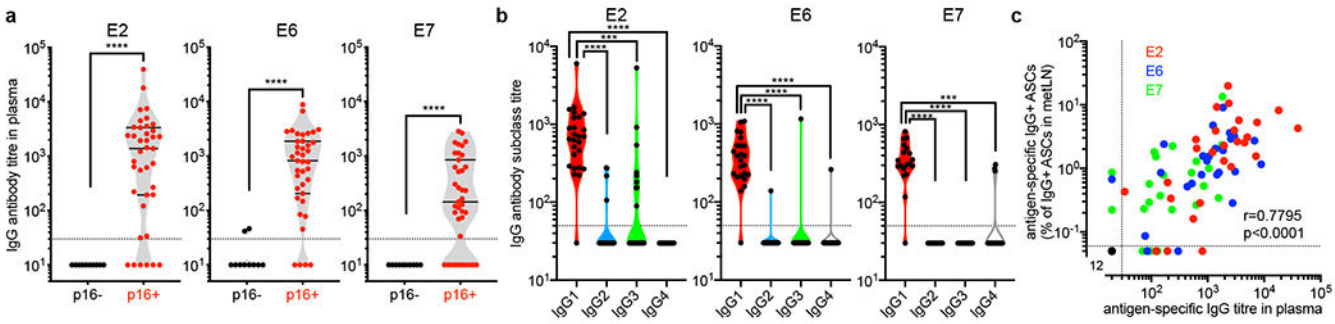

Figure 2. HPV-specific IgG antibody titres correlate with HPV-specific IgG-secreting cells in the TME.

a, E2/6/7-specific IgG plasma titres of p16- (n=10) and p16+ (n=39) HNSCC patients. Results with median and quartiles. Two-tailed Mann-Whitney with ****p<0.0001. **b,** IgG subclass titres against E2 (n=26), E6 (n=24), and E7 (n=19). Friedman test with two-sided Dunn's multiple comparisons test with ***p<0.001, and ****p<0.0001. **c,** Correlation (Spearman) between E2/6/7-specific IgG+ ASCs in metLN and E2/6/7-specific IgG plasma titres (n=30 patients).

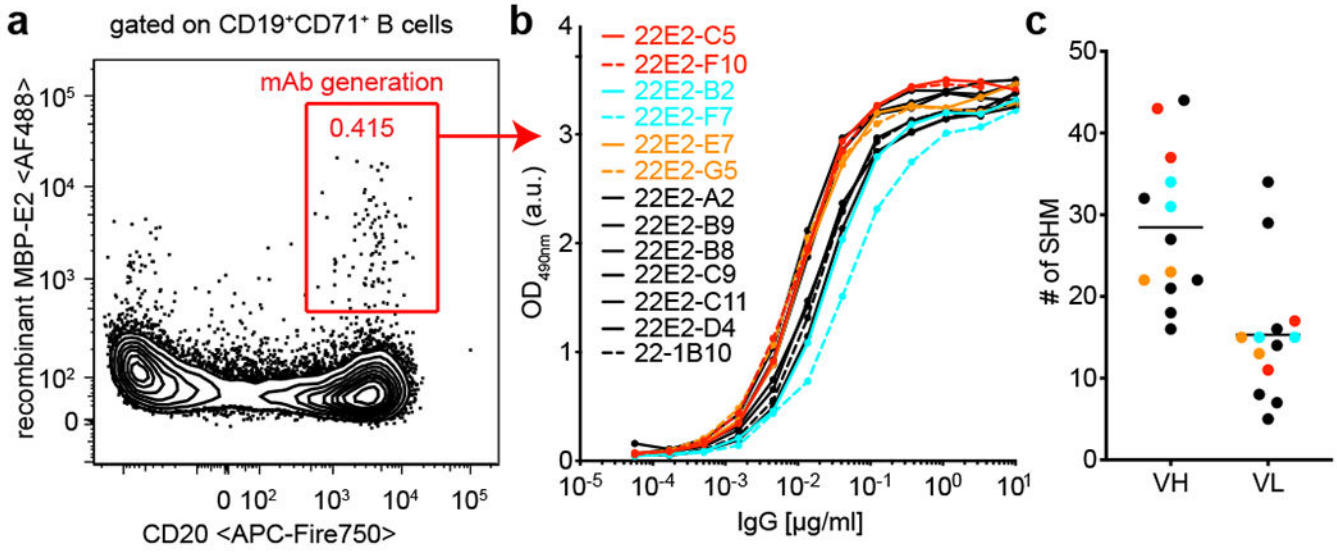

Figure 3. Generation of human monoclonal antibodies against HPV from HNSCC patients.

a, Flow plot showing E2-specific activated B cells ($CD3/14/16^{-}CD19^{+}CD20^{+}IgD^{-}CD71^{+}MBP\text{-}E2^{+}$) used for E2-specific mAb generation. **b,** ELISA of generated E2-specific mAbs (colours indicate clonally-related mAbs). arbitrary units (a.u.) **c,** Number of somatic hypermutations (SHM) in variable heavy (VH) and light (VL) chain of E2-specific mAbs (n=13) with indicated mean.

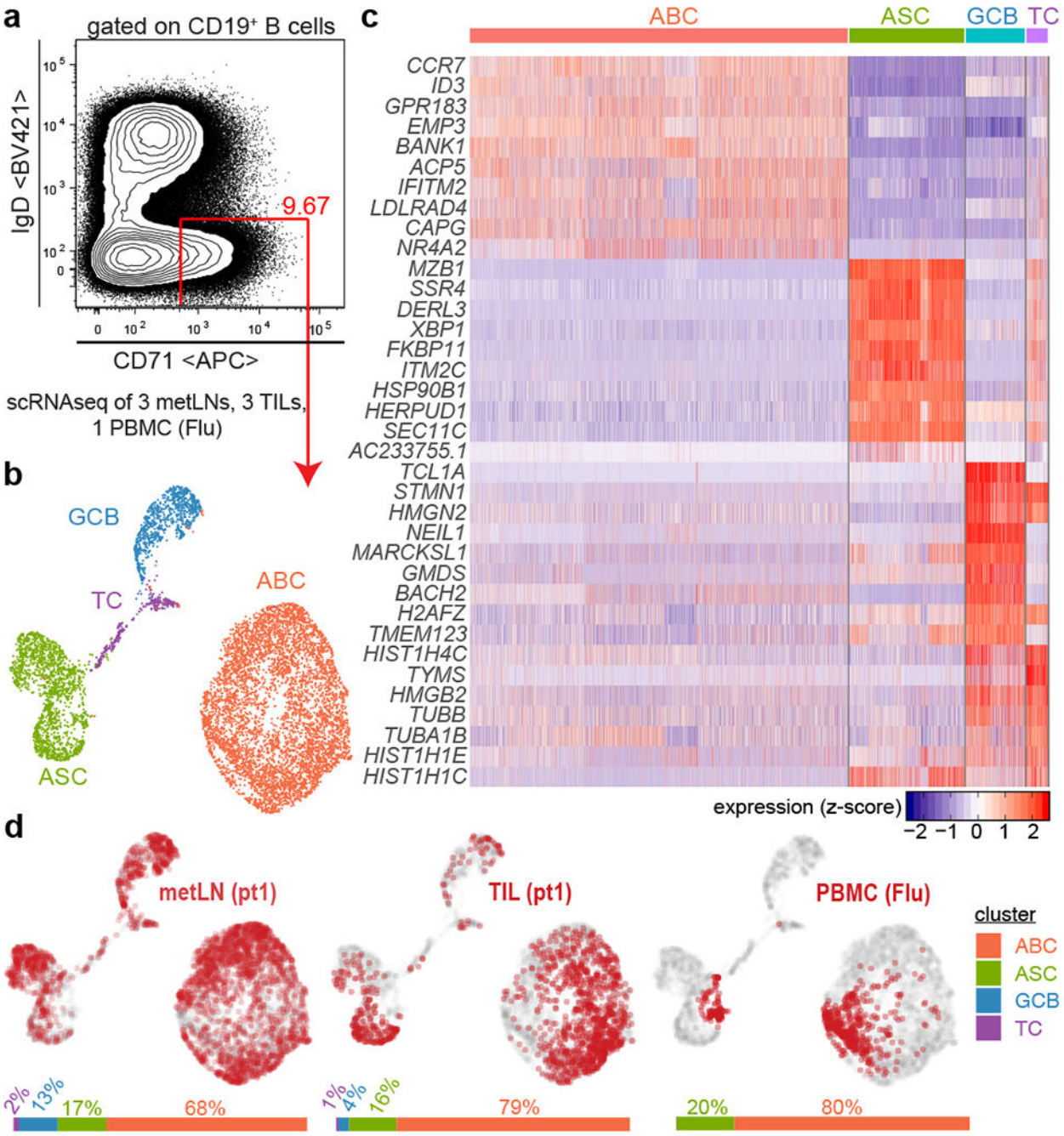

Figure 4. The tumour microenvironment contains activated B cells, germinal centre B cells and ASCs.

Activated B cell populations from metLN and TIL of 3 HPV+ HNSCC patients as well as PBMCs of an Influenza vaccinee were subjected to scRNA-seq. **a,** Flow plot of $CD19^{+}$ B cells from metLN showing activated $CD71^{high}$ cells (red gate). **b,** UMAP plot showing 4 identified clusters with cells obtained from PBMC (Flu), metLNs, and TILs. **c,** Heatmap showing relative expression of the top differentially expressed genes of each cluster. **d,**

UMAP plots showing distribution of cells of the indicated patient and tissue origin (in red) among the identified clusters.

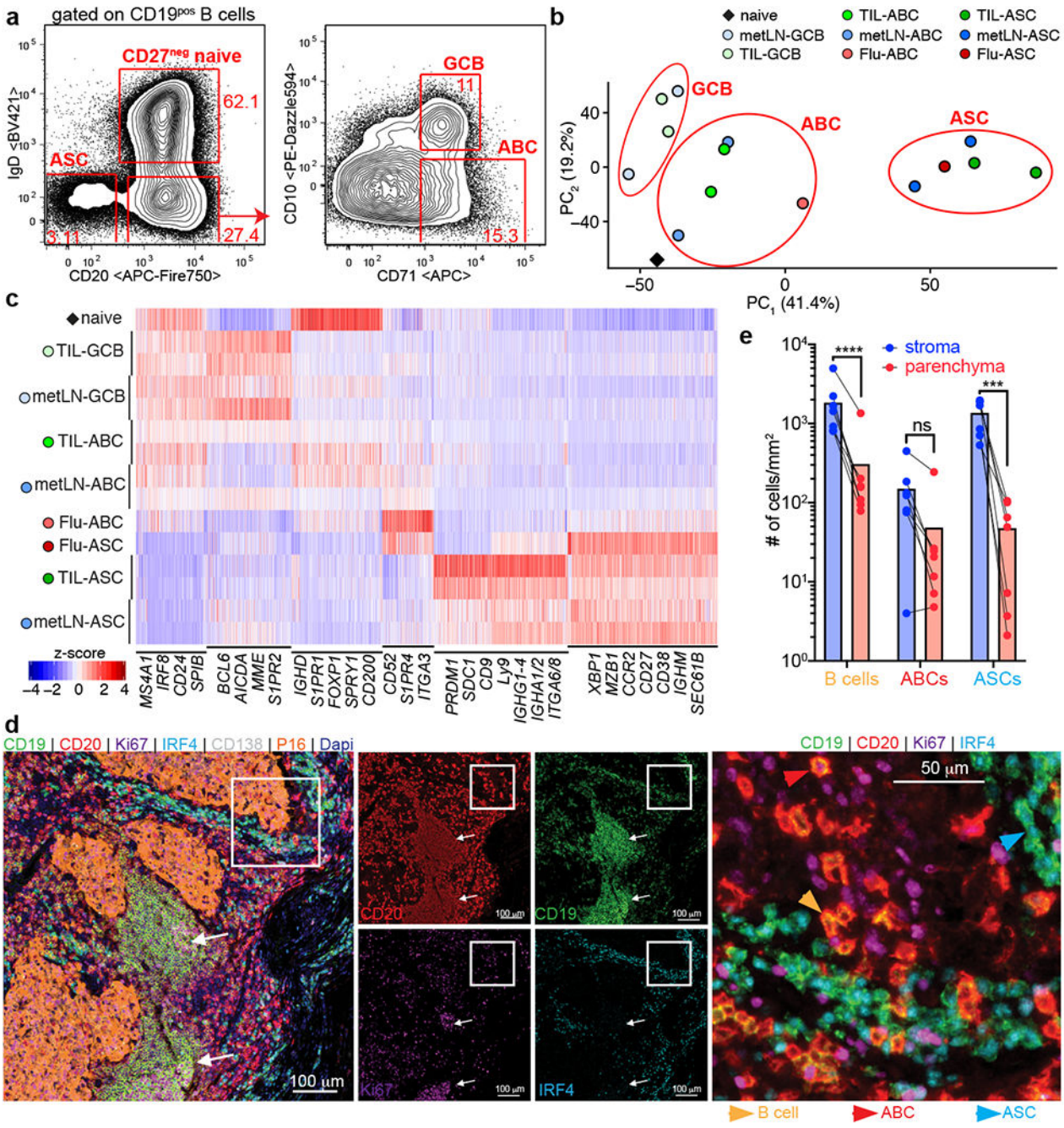

Figure 5. Transcriptomic and spatial characterisation of B cells and plasma cells in the tumour microenvironment.

a, Flow plots of CD19^{+} B cells from metLN highlighting the gating strategy for naïve B cells, ASCs, ABCs and GCBs for subsequent RNA-seq. **b,** Principal component analysis. **c,** Heatmap showing relative expression of differentially expressed genes across groups. Selected genes with high expression in individual clusters are indicated. **d,** Representative multiplex immunohistochemistry of HPV+ HNSCC tumours (n=7) with B cell infiltrates and associated germinal centres (white arrows). **e,** Quantification of B cells, ABCs, and ASCs in

stroma and p16+ tumour parenchyma of 7 HPV+ HNSCC patients. Two-way RM ANOVA with Sidak's multiple comparison with ***p<0.001, ****p<0.0001, ns not significant.